The International Journal of Advanced Manufacturing Technology (2019) 105:2513–2521
https://doi.org/10.1007/s00170-019-04485-5

ORIGINAL ARTICLE

# Study on magnetic abrasive finishing of AlSi10Mg alloy prepared by selective laser melting

Xiao Teng[1] · Guixiang Zhang[1] · Yugang Zhao[1] · Yuntao Cui[1] · Linguang Li[1] · Linzhi Jiang[1]

Received: 12 June 2019 / Accepted: 20 September 2019 / Published online: 1 November 2019


**Abstract**
Selective laser melting (SLM) technology is playing an increasingly important role in today's manufacturing industry. However, the surface quality of SLM samples is relatively poor and cannot be directly applied to industrial production. Therefore, this paper focuses on the post-treatment process of SLM AlSi10Mg alloy. First, the rough machining is performed by a grinding process (GP), and then, the magnetic abrasive finishing (MAF) is used for finish machining. The experiment results show that the combination of GP and MAF can effectively reduce the surface roughness and improve the surface quality of SLM AlSi10Mg alloy. The GP reduced the surface roughness to drop from 7 μm (after SLM forming) to about 0.6 μm, and the rough surface with defects such as spheroids and pits evolved into the fine surface with scratches and pores. The MAF reduced the surface roughness to a minimum of 0.155 μm, which resulted in excellent surface morphology. The surface hardness after the GP was higher, and the MAF reduced the hardness of the GP surface.

**Keywords** Selective laser melting · AlSi10Mg alloy · Grinding process · Magnetic abrasive finishing · Surface roughness · Hardness

## 1 Introduction

Nowadays, additive manufacturing technology has become an important symbol of the development level of a country's manufacturing industry. As an essential branch of additive manufacturing technology, SLM plays an increasingly important role in industrial production [1–3]. The forming process of SLM does not require any tools or fixtures, which can directly manufacture complex metal parts that cannot be produced by traditional machining methods, significantly shortening the manufacturing cycle of parts. However, in most practical applications, we need SLM parts to have a sufficiently good surface quality [4]. It is well known that the surface quality of SLM parts is relatively poor, which requires the surface treatment of the SLM parts to improve the surface quality.

Magnetic abrasive finishing (MAF) as the final processing of the workpiece has an important influence on the improvement of the surface quality [5, 6]. The free magnetic abrasives form a flexible magnetic brush, and the cutting edge of the tiny ceramic particles on the abrasive surface removes the surface of the workpiece slightly [7, 8]. Due to the good "self-adaptability" and "self-sharpening" of the abrasive particles, the MAF can be applied to a variety of occasions such as plane, round surface, complex surface, and small part, which is a very effective technology for improving surface quality [9–11].

International research on the surface treatment of SLM samples has gradually increased. Yung et al. [12] studied the application of laser polishing in additive manufacturing of CoCr alloys. The used of layered laser polishing method can significantly reduce the surface roughness of the complex surface and plane and improve the surface hardness. Zhang et al. [13] studied the electrochemical polishing of SLM Inconel 718 sample surface and analyzed the evolution of surface morphology and roughness during ECP. Duval-Chaneac et al. [14] performed abrasive flow machining on the SLM surface of heat-treated and non-heat-treated and studied the roughness evolution after finishing. The conclusion is that the higher the abrasive concentration and medium viscosity, the lower the surface roughness. Most of the research used the laser [12], electrochemistry [13], abrasive flow [14], machining [15], plasma spraying [16], and other processes to treat the

✉ Guixiang Zhang
zhanggx2013@163.com

[1] School of Mechanical Engineering, Shandong University of Technology, Zibo 255000, China

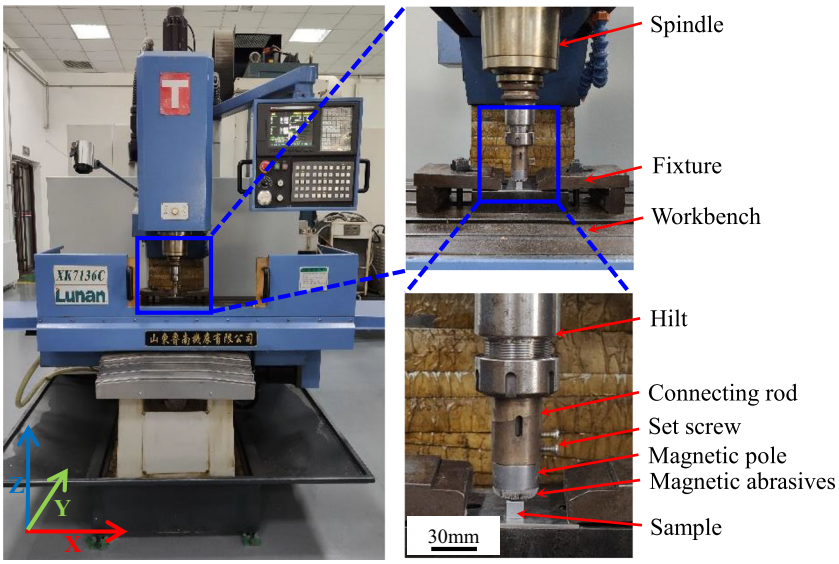


**Fig. 1** Magnetic abrasive finishing machine tool structure map

surface of the SLM samples. However, there are relatively few researches using MAF technique to improve the surface quality of SLM samples.

In this paper, the AlSi10Mg samples prepared by SLM are used for grinding process (GP) and magnetic abrasive finishing (MAF), carry out this experiment on the side of the SLM samples (parallel to the building direction), analyze the side forming mechanism of the SLM samples, and establish the side contour roughness model. The evolution of the surface roughness, surface morphology, and hardness of the SLM sample side during the MAF of three different types of magnetic abrasives was studied.

## 2 Experimental

### 2.1 Experimental equipment

Figure 1 shows the diagram of the magnetic abrasive finishing machine tool. The MAF experiment is carried out using the MAF device modified by the XK7136C CNC milling machine. The sample is placed on the workbench, clamped by the fixture, the magnetic pole is mounted on the connecting rod, and the magnetic abrasives are adsorbed on the magnetic pole, then the MAF can be carried out. During machining, the magnetic pole rotates with the spindle. The NdFeB permanent magnet material is used as the magnetic pole, and the NdFeB material is widely used because of its high coercive force and magnetic energy product. Moreover, the "✲ shape" groove is processed on the NdFeB magnetic pole, the groove width is 2 mm, and the depth is 2 mm, as shown in Fig. 2a. The groove of the magnetic pole causes uneven magnetic field on the surface of the magnetic pole, forming a magnetic field strength gradient, which helps to enhance the effect of MAF. It has been verified by the literature [17] that the "✲ shape" slotted magnetic pole has higher MAF efficiency than the unslotted magnetic pole. Due to the high brittleness and high hardness of NdFeB material, the groove type is generally processed by wire cutting. The maximum diameter of the magnetic pole is 28 mm and longitudinal magnetization is adopted. MAF is performed using SiC W7 (5–7 μm), SiC W40 (28–40 μm), $Al_2O_3$ W7 spherical magnetic abrasives

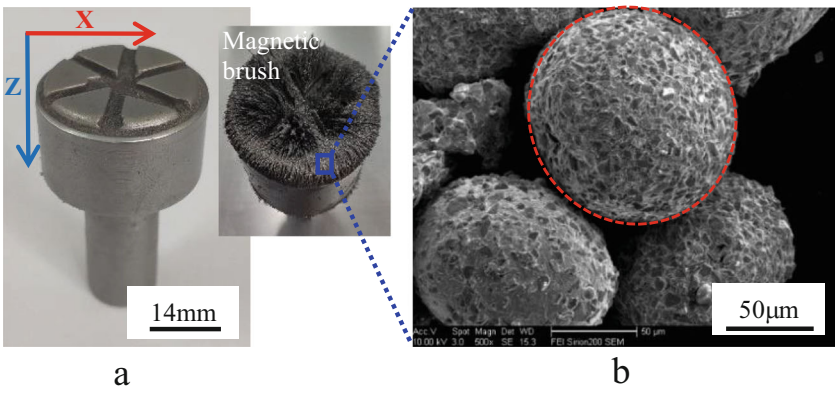


**Fig. 2** Magnetic pole adsorbing magnetic abrasives to form magnetic brush. **a** "✲ shape" NdFeB magnetic pole, **b** spherical magnetic abrasives

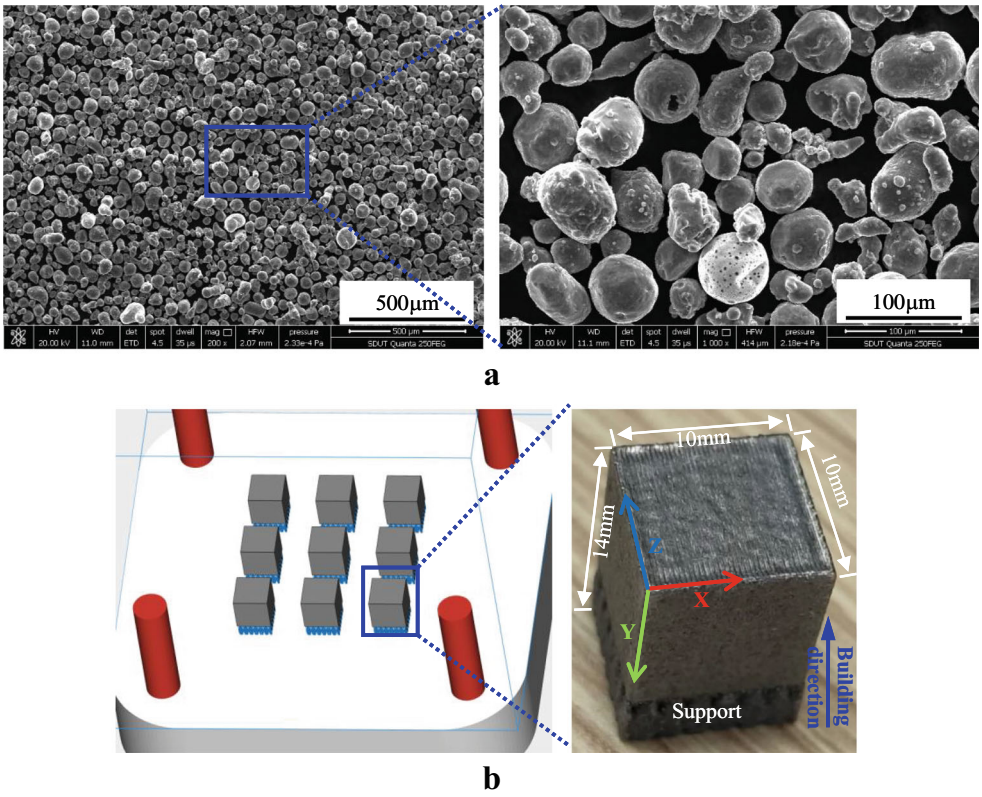


**Fig. 3** SLM molded AlSi10Mg samples. **a** SEM maps of AlSi10Mg powder; **b** SLM AlSi10Mg sample dimensions

prepared by gas atomization with rapid solidification, as shown in Fig. 2b. Magnetic abrasives prepared by gas atomization with rapid solidification have higher sphericity, better MAF effect, and longer service life [18, 19].

The AlSi10Mg powder with the particle size range of 20–63 μm was used as the SLM forming material. The microstructure of the powder was observed by scanning electron microscope (SEM), as shown in Fig. 3a. The higher sphericity of the powder indicates good fluidity and meets SLM forming requirements. The chemical composition of AlSi10Mg powder was analyzed by energy dispersive spectrometer (EDS). The chemical element content is shown in Table 1. The powder has a high purity and no other impurity elements.

The experimental samples were processed by SLM®125HL equipment (SLM®250HL, SLM Solutions GmbH, Germany). The samples were prepared using a 30-μm layer thickness and 67° rotation scanning strategy. The 4-mm support was added to facilitate the separation of the SLM samples from the platform. The SLM samples are shown in Fig. 3b.

The SLM forming process is complex, and the forming parameters are slightly different in different positions of the sample. The forming parameters inside the SLM samples (Hatch-Volume) are power = 350 W, speed = 1650 mm/s, focus = 0 mm, and each layer is scanned once. The forming parameters of the sample contour are different from the inside, and each layer is scanned twice. The forming parameters of fill contour-volume are power = 300 W, speed = 730 mm/s, and focus = − 4 mm. The forming parameters of border-volume are power = 300 W, speed = 730 mm/s, and focus = 0 mm.

**Table 1** Chemical element compositions of the AlSi10Mg powder

| Element | Al | Si | Mg |
|---|---|---|---|
| Weight% | 88.98 | 9.83 | 1.19 |

## 2.2 Experimental procedure

First of all, the vertical cross-section of the surface to be machined was taken. After electropolishing, the metallographic microscope (IE200M, SHUN YU, China) was used

**Table 2** AlSi10Mg samples grinding process (GP) parameters

| Experimental factor | Parameter |
|---|---|
| Grinding wheel abrasives type | $Al_2O_3$ series mixed abrasive |
| Grinding wheel binding agent | ceram |
| Particles size | 160–200 μm |
| Linear speed | 1400 m/min |
| Feed rate | 3 μm |
| Grinding depth | 40 μm |

**Table 3** AlSi10Mg sample MAF parameters

| Experimental factor | Parameter |
|---|---|
| Spindle speed | 1500 rpm |
| Machining gap | 2 mm |
| Outer edge linear speed | 1.96 m/s |
| Abrasive filling amount | 2.5 g |
| Magnetic abrasives type | Gas atomization SiC/$Al_2O_3$ magnetic abrasives |
| Magnetic abrasives average size | 75–150 μm |
| Abrasive particle phase size | W7 (5–7 μm)/W40 (28–40 μm) |
| Grinding fluid type | Oil-based grinding fluid |
| Grinding fluid supply amount | Add 0.2 ml every 3 min |
| Grinding fluid supply method | Graduated dropper |
| Magnetic pole type | Nd–Fe–B magnetic pole |

to observe the cross-section microscopic morphology, revealing the SLM forming principle of the cross-section. Since the surface of the SLM sample is rough, it is about Ra 7 μm. Before MAF, the CNC forming grinder (SMART-B818III, CHEVALIER, China) was used for grinding to reduce the surface roughness to about Ra 0.6 μm. The GP parameters of AlSi10Mg samples are shown in Table 2. Due to the easy oxidation of aluminum alloy, after each grinding, the sample is stored in the beaker containing anhydrous ethanol, and ultrasonic cleaner (SK2210HP, KUDOS, China) is used for 10 min to remove surface chips and other impurities; the samples were placed on a metallographic microscope (AXIO LAB A1, CARL ZEISS, Germany) to observe the surface morphology of the samples; the surface roughness of the samples was measured by roughness meter (TR-200, TIME, China); the surface hardness of the samples was measured by Vickers hardness tester (FM-800, FUTURE-TECH, Japan), the test load was 1000 gf, and the dwell time was 10 s. The MAF parameters of the AlSi10Mg samples are shown in Table 3.

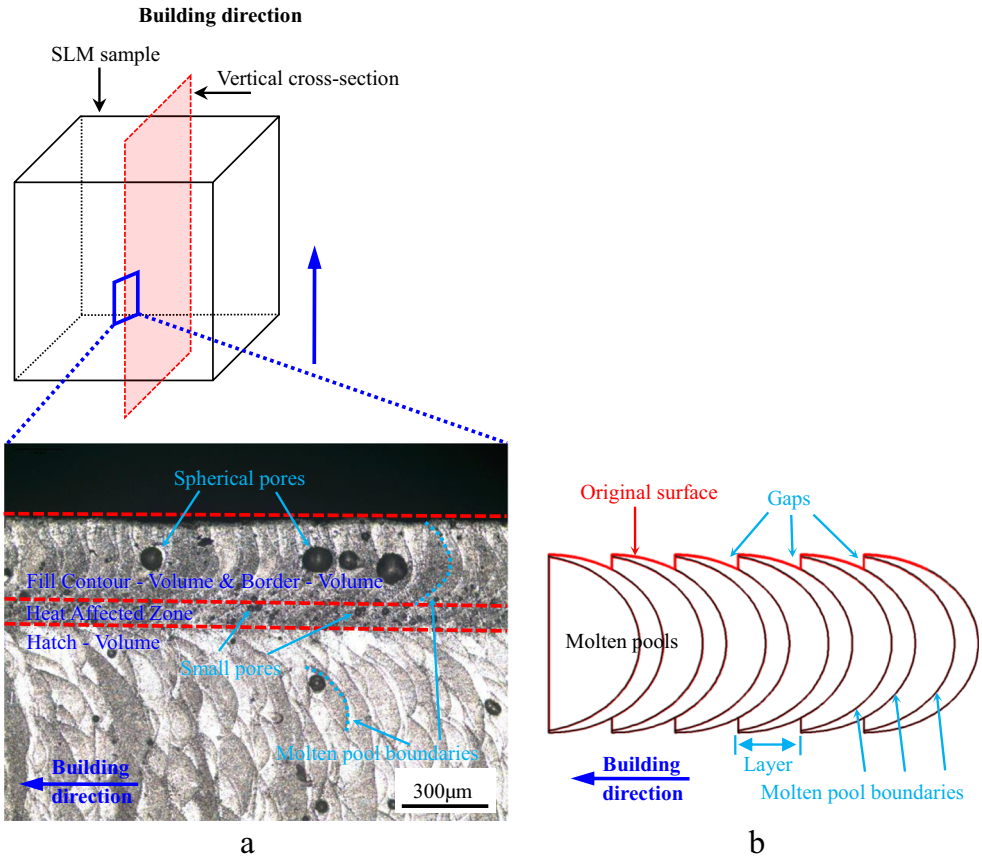


**Fig. 4** SLM sample contour forming strategy. **a** SLM sample vertical cross-section microstructure; **b** contour roughness model

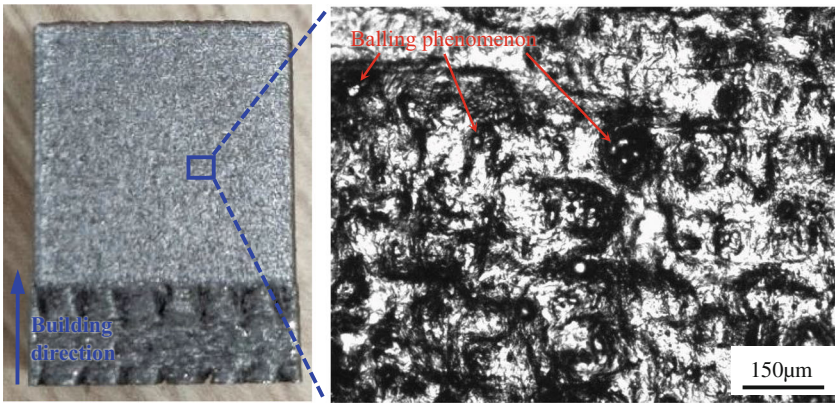


**Fig. 5** Surface micrograph of the SLM sample side

## 3 Results and discussion

### 3.1 Sample contour

Figure 4 shows the vertical cross-section microstructure and contour roughness model of SLM samples. It can be seen from Fig. 4a, the different microstructure is formed due to the differences in the internal and contour forming parameters of the sample. The spherical pores can be seen from the vertical cross-section, and the inside of the sample has fewer pores and small size. However, the pores on the contour are relatively more and larger in size. The contour of each layer is scanned twice, and the second scan produces laser remelting effect. Laser remelting can effectively improve surface texture and eliminate surface pores [20, 21]. However, the problem of low surface roughness is still present. As shown in Fig. 4b, there are still gaps between each layer, which is unavoidable, resulting in an uneven surface and increased roughness. Also, the phenomenon of surface spheroidization cannot be ignored, as shown in Fig. 5. These are the causes of low surface roughness and poor surface morphology.

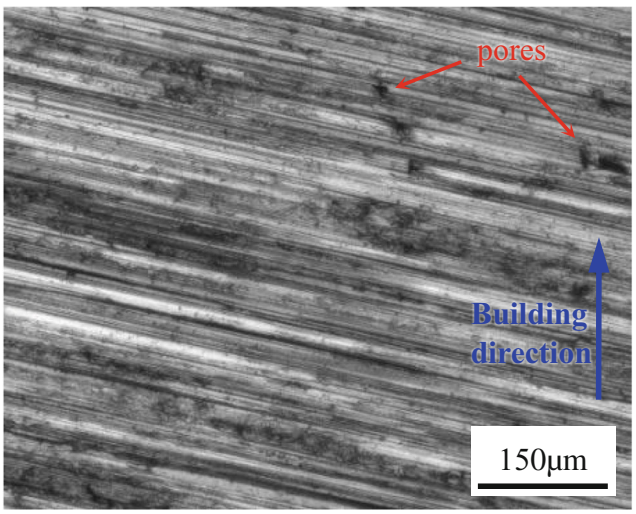


**Fig. 6** Surface micrograph after GP of SLM sample

### 3.2 Surface roughness and surface morphology

The surface roughness of the GP samples was Ra 0.596 μm for sample No. 1, Ra 0.627 μm for sample No. 2, and Ra 0.618 μm for sample No. 3. As can be seen from Fig. 6, the surface after the GP has a lot of scratches and pores. During the MAF, the surface roughness is measured every 3 min, and the magnetic abrasives are replaced every 12 min.

Figure 7 shows the effect of three different magnetic abrasives on surface roughness. It can be seen from the figure that the surface roughness of the first 9 min showed a sharp decline, the sample No. 1 (SiC W7) decreased from Ra 0.596 μm to Ra 0.222 μm; the sample No. 2 (SiC W40) decreased from Ra 0.627 μm to Ra 0.321 μm; the sample No. 3 ($Al_2O_3$ W7) achieved the lowest surface roughness at 9 min, which decreased from Ra 0.618 μm to Ra 0.194 μm. This is because, at the beginning of the MAF, there are a lot of burrs and pores on the surface of the sample, and the convex portion is subjected to a larger magnetic field force, so that the magnetic brush obtains sufficient

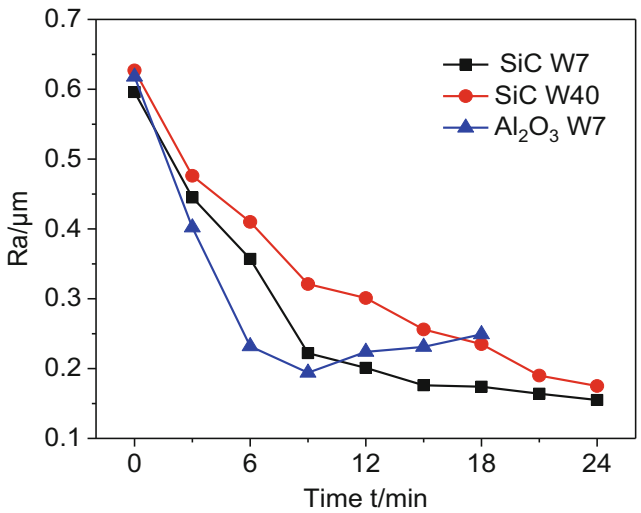


**Fig. 7** Change in surface roughness with time (outer edge linear speed = 1.96 m/s)

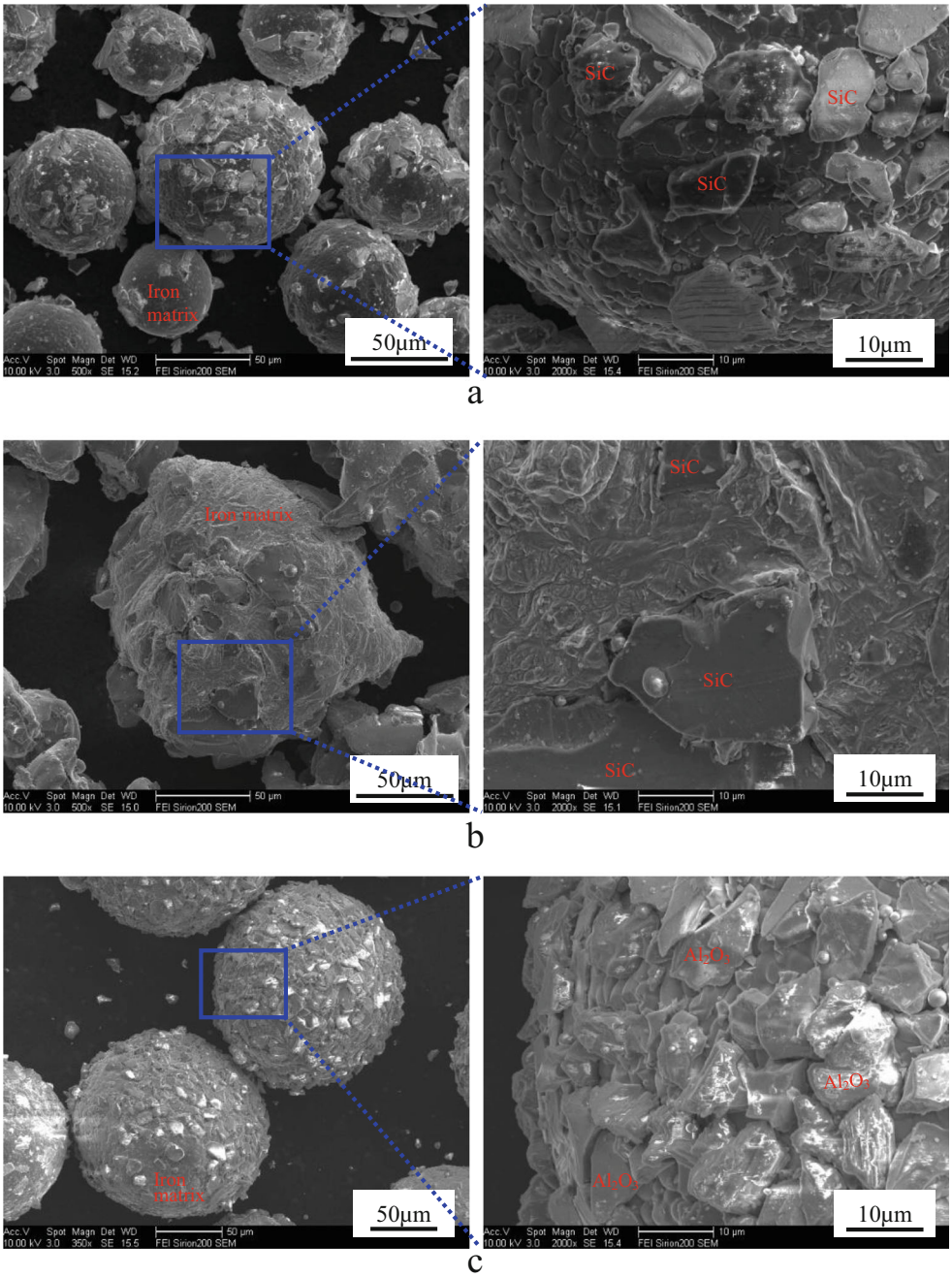


**Fig. 8** SEM maps of magnetic abrasives prepared by gas atomization with rapid solidification. **a** SiC W7 magnetic abrasives, **b** SiC W40 magnetic abrasives, **c** $Al_2O_3$ W7 magnetic abrasives

grinding pressure at the convex portion. The surface roughness of samples No. 1 and No. 2 was slightly reduced between 9 and 12 min. This is due to the passivation of the magnetic abrasives, and part of the abrasive particle phases is detached from the iron matrix, resulting in a slight decrease in grinding effect. The surface roughness of sample No. 3 has a reverse rise, because the preparation technique of the $Al_2O_3$ W7 magnetic abrasives used is relatively mature, as shown in Fig. 8c, compared with Fig. 8a, b, the surface of the iron matrix of $Al_2O_3$ W7 magnetic abrasives adheres to more abrasive particle phase, and the magnetic abrasives have higher sphericity, which basically conforms to the ideal spherical abrasive morphology. The iron matrix has good wettability with the abrasive particles, so that the MAF efficiency is higher, the magnetic abrasive life is longer, and the MAF effect is not significantly reduced in a short time. When the surface roughness is low, continuing the MAF will scratch the surface of the sample, which may cause the roughness to rise.

The new magnetic abrasives were replaced at 12 min, and the MAF was carried out for another 12 min, the roughness of samples No. 1 and No. 2 continued to decrease, dropping to the lowest roughness of Ra 0.155 μm and Ra 0.175 μm. The roughness of sample No. 3 continued to rise, and it was found

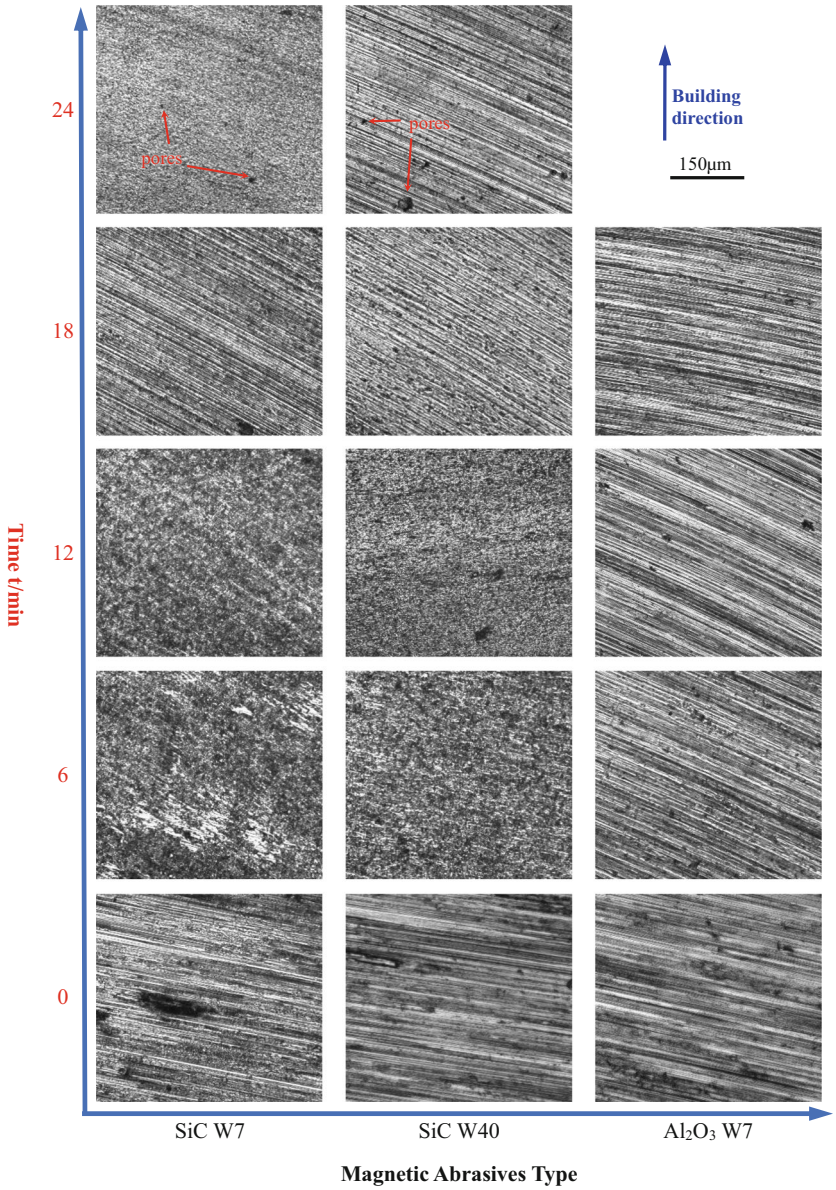


**Fig. 9** Evolution of surface micrograph of different types of magnetic abrasives during MAF

that there was a significant concave in the grinding at 18 min. This is due to the fact that magnetic abrasives have a higher grinding efficiency, and when the grinding time is too long, the material removal amount is too large. This phenomenon did not occur in samples No. 1 and 2.

Figure 9 shows the evolution of the surface morphology during the MAF process. The samples No. 1 and No. 2 had basically eliminated the scratches generated by the GP when the MAF was performed for 12 min, and the surface texture was good. At this time, the surface roughness was significantly reduced; as shown in Fig. 7, the surface roughness decreased by 89.5% and 68.8% in 12 min, respectively. At 18 min, the new scratches caused by MAF were found. Due to the low hardness of the aluminum alloy, the material has poor resistance to plastic deformation or scratches, and the MAF is more likely to scratch the surface of the sample. These scratches were shallow, and the surface roughness was still declining. The scratches were reduced at 24 min, but they were still present, and the surface roughness reached the lowest values of Ra 0.155 μm and Ra 0.175 μm respectively, as shown in Fig. 7. The $Al_2O_3$ W7 magnetic abrasives used in the No. 3 sample are better, whether it is the number of abrasive particles on the iron matrix or the combination of the two, so the MAF effect is stronger. At 6 min, the scratches caused by the GP were removed, and a new texture was produced, achieving the minimum roughness of Ra 0.194 at 9 min, as shown in Fig. 7.

### 3.3 Vickers hardness test

Figure 10 shows the evolution of Vickers hardness during MAF. The Vickers hardness of the surface after GP was

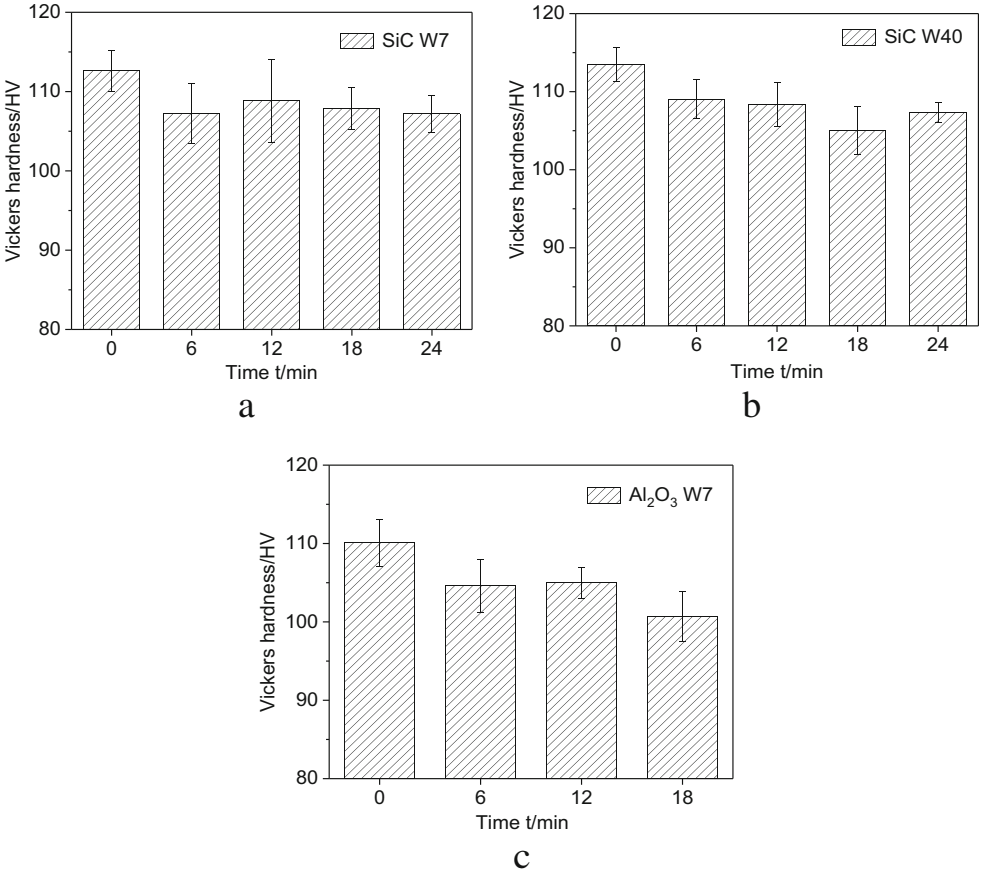


**Fig. 10** Evolution of Vickers hardness of different types of magnetic abrasives during MAF. **a** SiC W7, **b** SiC W40, **c** $Al_2O_3$ W7

112.6 HV, 113.5 HV, and 110.1 HV. It can be seen from the figure that the Vickers hardness of the surface after GP is higher than the MAF, which is due to the work hardening effect of the sample during the GP [22]. At the same time, the GP also causes lattice distortion, which increases the internal energy of the material, hinders the dislocation slip deformation, and plays a certain hardness strengthening effect [23]. After MAF for 6 min, the Vickers hardness value caused a sharp drop, which is due to the removal of the material resulting in the shallowing of the work-hardened layer and the release of internal energy [24]. With the prolongation of the MAF time, the Vickers hardness value has slightly fluctuated, but it is basically stable. Because the cutting force of the MAF is small, the surface hardness is not greatly affected.

It is found from Fig. 10c that the Vickers hardness decreased sharply from 105 HV at 12 min to 100.7 HV at 18 min. This is due to the higher grinding efficiency resulting in more material removal. The detection found that the depth of the grinding has exceeded the contour of the sample.

To this end, the contour, heat-affected zone (HAZ), and inside hardness were measured on the vertical cross-section of the sample, as shown in Fig. 4a. The hardness of the sample contour (fill contour-volume and border-volume) was 111.8 HV, the hardness of the HAZ was 101.5 HV, and the hardness of the inside (hatch-volume) was 113.6 HV. Thus, in Fig. 10c, the hardness measured at 18 min is the hardness of the HAZ. According to the literature [25], the hardness experiment and microstructure observation of the molten pool of SLM AlSi10Mg alloy were carried out, and the conclusion that the hardness at the boundary of the molten pool was lower than the inside. The HAZ is located at the junction of the molten pool boundary of the sample contour and the sample inside, which causes the hardness to decrease. As can be seen from Fig. 4a, the HAZ has some small pores, which also reduces the HAZ hardness.

## 4 Conclusion

In this paper, the SLM AlSi10Mg alloy is polished by a combination of grinding process (GP) and magnetic abrasive finishing (MAF). The GP uses 160–200 μm $Al_2O_3$ series mixed abrasives, and the MAF uses SiC W7, SiC W40, $Al_2O_3$ W7 spherical magnetic abrasives prepared by gas atomization with rapid solidification. The results show that: the surface roughness of the samples after GP is about 0.6 μm, and there are many scratches and pores. After that, MAF is performed. Good results are obtained by MAF using three kinds of magnetic abrasives. The lowest surface roughness of 0.155 μm is obtained by SiC W7 magnetic abrasive

machining, and the surface morphology is good. The surface roughness of the $Al_2O_3$ W7 magnetic abrasive machining decreases the fastest, which depends on the number of abrasive particles adhered to the surface of the magnetic abrasives and the degree of adhesion between the abrasive particles and the iron matrix. The combination of GP and MAF can effectively reduce the surface roughness of SLM AlSi10Mg alloy and improve surface quality.

Also, the surface hardness of the sample after the GP is high, mainly caused by work hardening and lattice distortion. The MAF makes the work-hardened layer shallow, releasing the internal energy of the material, thereby reducing the hardness.

**Funding information** This research was funded by National Natural Science Fundation of China (Grant number 51675316).

## References


1. Zhang D, Zhang P, Liu Z, Feng Z, Wang C, Guo Y (2018) Thermofluid field of molten pool and its effects during selective laser melting (SLM) of Inconel 718 alloy. Addit Manuf 21:567–578. https://doi.org/10.1016/j.addma.2018.03.031
2. Li W, Li S, Liu J, Zhang A, Zhou Y, Wei Q, Yan C, Shi Y (2016) Effect of heat treatment on AlSi10Mg alloy fabricated by selective laser melting: Microstructure evolution, mechanical properties and fracture mechanism. Mater Sci Eng A 663:116–125. https://doi.org/10.1016/j.msea.2016.03.088
3. Wei P, Wei Z, Chen Z, Du J, He Y, Li J, Zhou Y (2017) The AlSi10Mg samples produced by selective laser melting: single track, densification, microstructure and mechanical behavior. Appl Surf Sci 408:38–50. https://doi.org/10.1016/j.apsusc.2017.02.215
4. Coz GL, Fischer M, Piquard R, D'Acunto A, Laheurte P, Dudzinski D (2017) Micro cutting of Ti-6Al-4V parts produced by SLM process. Procedia CIRP 58:228–232. https://doi.org/10.1016/j.procir.2017.03.326
5. Wu J, Zou Y, Sugiyama H (2015) Study on finish characteristics of magnetic abrasive finishing process using low-frequency alternating magnetic field. Int J Adv Manuf Technol 85:585–594. https://doi.org/10.1007/s00170-015-7962-9
6. Zhang G (2012) Study on preparation of magnetic abrasives by gas atomization with rapid solidification and their finishing performance. Nanjing University of Aeronautics and Astronautics http://cdmd.cnki.com.cn/Article/CDMD-10287-1014060820.htm
7. Zou Y, Xie H, Dong C, Wu J (2018) Study on complex micro surface finishing of alumina ceramic by the magnetic abrasive finishing process using alternating magnetic field. Int J Adv Manuf Technol 97:2193–2202. https://doi.org/10.1007/s00170-018-2064-0
8. Jiao AY, Quan HJ, Li ZZ, Zou YH (2015) Study on improving the trajectory to elevate the surface quality of plane magnetic abrasive finishing. Int J Adv Manuf Technol 80:1613–1623. https://doi.org/10.1007/s00170-015-7136-9
9. Zhang G, Zhao Y, Zhao D, Zuo D, Yin F (2013) New iron-based SiC spherical composite magnetic abrasive for magnetic abrasive finishing. Chin J Mech Eng 26:377–383. https://doi.org/10.3901/CJME.2013.02.377
10. Zhang GX, Zhao YG, Zhao DB, Yin FS, Zhao ZD (2011) Preparation of white alumina spherical composite magnetic abrasive by gas atomization and rapid solidification. Scr Mater 65(5):416–419. https://doi.org/10.1016/j.scriptamat.2011.05.021
11. Du ZW, Chen Y, Zhou K, Li C (2015) Research on the electrolytic-magnetic abrasive finishing of nickel-based superalloy GH4169. Int J Adv Manuf Technol 81:897–903. https://doi.org/10.1007/s00170-015-7270-4
12. Yung KC, Xiao TY, Choy HS, Wang WJ, Cai ZX (2018) Laser polishing of additive manufactured CoCr alloy components with complex surface geometry. J Mater Process Technol 262:53–64. https://doi.org/10.1016/j.jmatprotec.2018.06.019
13. Zhang B, Li X, Bai J, Guo J, Wang P, Sun C, Nai M, Qi G, Wei J (2016) Study of selective laser melting (SLM) Inconel 718 part surface improvement by electrochemical polishing. Mater Des 116:531–537. https://doi.org/10.1016/j.matdes.2016.11.103
14. Duval-Chaneac MS, Han S, Claudin C, Salvatore F, Bajolet J, Rech J (2018) Experimental study on finishing of internal laser melting (SLM) surface with abrasive flow machining (AFM). Precis Eng 54:1–6. https://doi.org/10.1016/j.precisioneng.2018.03.006
15. Yusuf K, Emre T (2018) Finish machining-induced surface roughness, microhardness and XRD analysis of selective laser melted Inconel 718 alloy. Procedia CIRP 71:500–504. https://doi.org/10.1016/j.procir.2018.05.013
16. Zhang B, Zhu L, Liao H, Coddet C (2012) Improvement of surface properties of SLM parts by atmospheric plasma spraying coating. Appl Surf Sci 263:777–782. https://doi.org/10.1016/j.apsusc.2012.09.170
17. Zhang P, Zhang G (2011) Design of a plane magnetic abrasive finishing device and the magnetic pole. J Shandong Univ Technol 25(6):67–70. https://doi.org/10.13367/j.cnki.sdgc.2011.06.010
18. Gao Y, Zhao Y, Zhang G (2018) Preparation of $Al_2O_3$ magnetic abrasives by gas-solid two-phase double-stage atomization and rapid solidification. Mater Lett 215:300–304. https://doi.org/10.1016/j.matlet.2017.12.124
19. Liang W, Zhang G, Zhang P, Jiang L, Qin P, Liang J, Teng X (2018) Experimental research on magnetic abrasive finishing for ZrO2 ceramic materials. Surf Technol 47(09):310–316. https://doi.org/10.16490/j.cnki.issn.1001-3660.2018.09.041
20. Yang Z, Guo Y, Xia F, Duan H, Gao P, Li J (2015) Effect of laser remelting treatment on microstructure and tensile property of piston aluminum alloy. Trans Mater Heat Treat 36(08):49–55. https://doi.org/10.13289/j.issn.1009-6264.2015.08.010
21. Zhang W (2015) Research on microstructure and hardness of Tin-base babbitt alloy made by laser remelting. Rare Metals 44(08):32–34. https://doi.org/10.14158/j.cnki.1001-3814.2015.08.009
22. Zhang H, Cheng R (2018) Influence of grinding process on microstructure and properties of ZL102 aluminum alloy. Aluminium Fabr 06:57–60. https://doi.org/10.3969/j.issn.1005-4898.2018.06.12
23. Zhao L (2019) Analysis of surface layer properties of aluminum alloy prestressed ultrasonic peen forming parts. Aerospace Manuf Technol 01:22–26 http://g.wanfangdata.com.cn/details/detail.do?_type=perio&id=htgy201901005
24. Xu H, Liu Y, Bu M, Cui F (2017) Experiment on surface work-hardening of spline by high speed cold roll-beating. Forging Stamping Technol 42(03):165–169. https://doi.org/10.13330/j.issn.1000-3940.2017.03.031
25. Teng X, Zhang G, Liang J, Li H, Liu Q, Cui Y, Cui T, Jiang L (2019) Parameter optimization and microhardness experiment of AlSi10Mg alloy prepared by selective laser melting. Mater Res Express 6:086592. https://doi.org/10.1088/2053-1591/ab18d0